

A Capacitor Model of the Helical Deflector: Revisiting Shamaev's Proposal and the Textbook Model

Hayk Lekdar Gevorgyan^{1,2*}

¹*Experimental Physics Division, Alikhanyan National Laboratory (Yerevan Physics Institute),*

²*2 Alikhanyan Brothers St., 0036 Yerevan, Armenia*

²*Quantum Technologies Division, Alikhanyan National Laboratory (Yerevan Physics Institute),*

²*2 Alikhanyan Brothers St., 0036 Yerevan, Armenia*

(Dated: January 16, 2026)

An RF helical deflector^a is a type of electron and ion optics device that applies a time-dependent rotating transverse electric or magnetic field by means of time-dependent RF voltage applied on two opposite conducting helical structures (wires, ribbons or other) to deflect charged particles (a single, bunch or beam) in a circular or spiral path. It is a perspective indirect timing system being concurrent for reaching picosecond time resolution, and have promise being excellent candidate for high precision time-of-flight detection. As a timing system, it converts the temporal structure of an electron beam into a spatial pattern — particularly, an ellipse in the case of a single-frequency RF voltage and continuous electron pencil beam.

I propose a *capacitor model* of an RF helical deflector and compare it with the existing *textbook model* [1, 2], interpret them and provide understanding of them. Furthermore, I analyze the latter, finding analytical formulas for the applied electric field, ellipse sizes (semi-axes) and rotation angle, lengths of the ellipse line, corresponding to the duration of electron pencil bunches or beams. The present article touches the topics of getting circle on resonance limit and of deflection sensitivity.

I. INTRODUCTION

Atomic clocks [3], while providing the most stable long-term time reference with an internal and absolute standard based on atomic transition frequencies, do not directly deliver picosecond-resolved absolute timestamps. In contrast, RF helical deflectors, as phase-referenced (indirect) timing systems using an RF field as the reference clock, can resolve picosecond-scale relative arrival times. Importantly, there is a huge difference — RF helical deflectors don't "tell time" in the same way as a clock — they don't have absolute timing yet like a clock, but they can resolve relative timing, measuring the relative arrival time of a charged particle within a picosecond time window [2].

From the other hand the most renowned direct timing systems are streak cameras, Time-to-Digital Converters (TDCs), RF deflectors, and frequency combs. Streak cameras measure ultrafast photon arrival times from optical, UV, X-ray, or sometimes visible light regions, by means of photocathode, electrostatic deflection plates with a time-varying fast ramp voltage and photoelectron detector. TDCs measure electronic pulse arrival times by digitizing time intervals: combining the coarse timestamp from the fast digital counter driven by a high-frequency electronic clock and the fine timing offset from the delay line/interpolator. In frequency combs, being "rulers in time", the event arrival time is measured with respect to known time markers, e.g., phase-coherent comb pulses, phase-locked to a stable RF or microwave

clock, which itself can be referenced to an atomic clock.

From the perspective of time-of-flight (TOF) and arrival time detection in electron optics, both streak cameras, RF deflectors, and electrostatic or magnetic TOF systems have an important role. All these systems have one in common — they use deflection mechanisms and can stand as mass spectrometers (limited to electrons in streak cameras), since the deflection of a charged particle depend on its velocity and mass-to-charge ratio. Deflection mechanisms are electrostatic field in electrostatic TOFs, static magnetic field in magnetic TOFs, electrostatic deflection plates in streak cameras, and RF oscillating electric field in RF deflectors. Two common types of RF deflectors are linear RF deflectors and RF helical deflectors. In the former, two parallel or cylindrical [4] electrodes are used to generate an oscillating transverse electric field which is standing in space and linearly polarized, producing a linear deflection in a fixed transverse direction. In the latter, a helically wound electrode (wire or ribbon) creates a traveling and rotating transverse RF field along the beam axis, resulting in a non-uniform helical deflection of the charged particles. In the present article, I show that the helical/circular polarization attributed to this rotating field in the *textbook model* [1, 2] is only a rough approximation and has a limited validity range.

Metallic helical structure systems are multifunctional being used both as helical undulators [5], helical waveguides [6–8], helical resonators [9–11], helical antennas [12], helical deflectors [2, 13], etc. Helical slow-wave structures are widely used as effective broadband transmission lines [14–17], helical resonators [18, 19], helical conductors [20].

The present article is devoted to the theoretical framework and applications of an RF helical deflector as a tim-

* hayk.gevorgyan@aanl.am

^a Note that this is not a final version, and the manuscript should be carefully reviewed before submission to any journal.

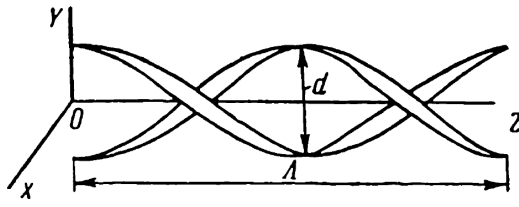


FIG. 1: Self-unfolding deflection system (helical deflector of charged particles).

ing system, a time-of-flight detector for charged particles, and a mass spectrometer.

The paper is organized as follows. In Sec. II, I provide a *capacitor model* of the helical deflector and explain the *textbook model* [1, 2]. Sec. III provides theoretical framework and method for measuring deflection transverse velocities and coordinates, ellipse sizes, its rotation angle. Sec. IV analyzes the limit $\omega \rightarrow \omega_c$, the deflection characteristics, and their comparison in three cases: 1) TOF measured at a screen immediately after the deflector, 2) TOF between the deflector and a screen, assuming that the charged particle leaves the deflector exactly from the axis, 3) total TOF, valid under the paraxial approximation inside the deflector. Here, *screen* refers to any target intercepted by the charged particles, representing a detector — for example, a multichannel plate. Secs. V, VI, VIII provide information on the problem of getting circle, the case of *on and off* pencil beam, the deflection sensitivity measures. Finally, Sec. IX represents comments and conclusions.

II. A CAPACITOR MODEL

In 1961, Yu. M. Shamaev proposed a self-unfolding deflection system for the oscillographic observation of UHF (ultrahigh frequency) processes, representing a section of two-wire line wound into a spiral [1, 2] (see Fig. 1).

A. Deflector field

Equation of helix is

$$x = R \cos \varphi, \quad y = R \sin \varphi, \quad z = R\kappa\varphi = \frac{\lambda}{2\pi}\varphi, \quad (1)$$

where $\lambda = l/n$ is a winding pitch of an helix (a solenoidal electrode) — the axial distance between the two ends of a single turn in a helical winding, where l is the axial distance between the ends of helix, n is the number of turns and can be fractional, $\kappa = \cot \psi = \lambda/(2\pi R)$, ψ is a winding pitch angle. When φ increases by 2π , z increases by λ or $2\pi R \cot \psi$, where R is the radius of helix and ψ is the angle of unfolded helix between directions of its axis and linear progression. Note that the length of the helix is $L = l/\cos \psi = n\sqrt{\lambda^2 + (2\pi R)^2}$.

The components of the radius vector \mathbf{r} and of the infinitesimal element of length ds are

$$r_x = x_0 - x = x_0 - R \cos \varphi, \quad ds_x = dx = -R \sin \varphi d\varphi, \quad (2a)$$

$$r_y = y_0 - y = y_0 - R \sin \varphi, \quad ds_y = dy = R \cos \varphi d\varphi, \quad (2b)$$

$$r_z = z_0 - z = z_0 - R\kappa\varphi, \quad ds_z = dz = R\kappa d\varphi, \quad (2c)$$

Using Coulomb's law and assuming that the charge density, arising from a capacitor's negative charge distribution, is uniform $dq(t) = -\rho(t)ds$, the electric field $\mathbf{E}(t)$ at a point can be expressed as:

$$\mathbf{E}(t) = - \int \frac{\rho(t)\mathbf{r}}{4\pi\epsilon_0 r^3} ds, \quad (3)$$

where $\rho(t)$ is the time-dependent linear charge density, \mathbf{r} is the position vector from the charge element to the observation point, $r = |\mathbf{r}|$ is its magnitude, ds represents an infinitesimal element of length, and ϵ_0 is the permittivity of free space. Eqs. (1), (2), (3) can be viewed as a *helical line approximation*.

Under the paraxial approximation $x_0 \approx y_0 \approx 0$, the expressions for radius vector $\mathbf{r} = r_x \mathbf{e}_x + r_y \mathbf{e}_y + r_z \mathbf{e}_z$, radius $r = \sqrt{r_x^2 + r_y^2 + r_z^2} = \sqrt{R^2 + (z_0 - R\varphi\kappa)^2}$ and length element $ds = \sqrt{ds_x^2 + ds_y^2 + ds_z^2} = R\sqrt{1 + \kappa^2}d\varphi$ from Forms. (2), the electric field vector can be written

$$\mathbf{E}(t) = \int_{\varphi_1}^{\varphi_2} Q(t)/R \left\{ \begin{array}{c} \cos \varphi \\ \sin \varphi \\ \kappa\varphi - z_0/R \end{array} \right\} \frac{d\varphi}{\left(1 + (z_0/R - \kappa\varphi)^2\right)^{3/2}} \quad (4)$$

Note that in the non-paraxial theory, the expression (4) for the electric field vector changes to

$$\begin{aligned} \mathbf{E}(t) &= \int_{\varphi_1}^{\varphi_2} Q(t)/R \left\{ \begin{array}{c} \cos \varphi - x_0/R \\ \sin \varphi - y_0/R \\ \kappa\varphi - z_0/R \end{array} \right\} \frac{d\varphi}{S(x_0, y_0, z_0, \varphi)}, \\ S(x_0, y_0, z_0, \varphi) &= \left(\left(\frac{x_0}{R} - \cos \varphi \right)^2 + \left(\frac{y_0}{R} - \sin \varphi \right)^2 + \left(\frac{z_0}{R} - \kappa\varphi \right)^2 \right)^{3/2}. \end{aligned} \quad (5)$$

Since the applied voltage $U(t) = U_0 \sin(\omega t + \phi)$ is periodic with a frequency ω and a phase ϕ , the linear charge density is also time-dependent given by the same law $\rho(t) = \rho_0 \sin(\omega t + \phi)$, hence, $Q(t) = Q_0 \sin(\omega t + \phi)$, where $Q_0 = 2\rho_0 \sqrt{1 + \kappa^2}/(4\pi\epsilon_0)$, where factor of 2 is taken into account since two helical electrodes create electric field which is twice the electric field generated in a single electrode with capacitance equivalent to linear charge density $\rho(t)$, and $\mathbf{E}(t) = \tilde{\mathbf{E}}(z_0) \sin(\omega t + \phi)$, where the formula (4) is the same for $\mathbf{E}(z_0)$ but Q_0 is taken instead of $Q(t)$, and we named $\tilde{\mathbf{E}}(z_0)$ as phasor electric field or phasor with analogy to electromagnetism and optics.

The linear charge density ρ_0 and capacitance density (per unit length) C of a two-wire line are given by

$$\rho_0 = CU_0, \quad C = \frac{\pi\epsilon_0\epsilon_d}{\ln \frac{d-b}{b}}, \quad (6)$$

where $d = 2R$ is the center-to-center distance between the wires, b is the radius of a single wire, ϵ_0 is the permittivity of free space (vacuum), ϵ_d is the relative permittivity of the dielectric between wires. Eqs. (4), (5), (6) are valid in a *helical line approximation*, i.e., when $b \ll d$.

B. Equations of motion

The equations of motion, using relativistic Lorentz force formula, follows

$$\frac{d\mathbf{v}}{dt} = -\frac{e}{m\gamma} (\mathbf{E}(t) + \mathbf{v} \times \mathbf{B}(t)), \quad (7)$$

where m is mass, e is absolute charge, $\gamma = 1/\sqrt{1+v^2/c^2}$ is Lorentz factor, $v = \sqrt{v_x^2 + v_y^2 + v_z^2}$ is velocity of an electron; $\mathbf{E}(t)$ and $\mathbf{B}(t)$ are applied electric and magnetic fields.

The paraxial approximation, which describes the motion of an electron near its beam axis, assumes that the longitudinal velocity, aligned with the beam axis, is relativistic (approaching the speed of light), while the transverse velocities remain significantly smaller in comparison. Assuming the zero initial transverse velocities $v_x(0) \approx v_y(0) \approx 0$ and the paraxial approximation $\Delta v_x \approx \Delta v_y \approx \Delta v_z \ll v_z$, one gets

$$\begin{aligned} \dot{v}_x &\approx -\frac{e}{m\gamma} (E_x(t) - v_z B_y(t)), \\ \dot{v}_y &\approx -\frac{e}{m\gamma} (E_y(t) + v_z B_x(t)), \\ \dot{v}_z &\approx 0, \end{aligned} \quad (8)$$

where $\gamma \approx 1/\sqrt{1+v_z^2/c^2}$. In more detail, in Eq. (8) used the fact that, since, the field components are of the same order $E_x(t) \approx E_y(t) \approx E_z(t)$ (and $B_x(t) \approx B_y(t) \approx B_z(t)$), the velocity changes also will be of the same order and much smaller than the longitudinal velocity $v_z \approx v_z(0) = \text{const}$. Since a change of the longitudinal component is much smaller compared to its initial value, the main cause of a change in the case of electric field $E_z(t)$ can be neglected (a *low longitudinal field* or, more precisely, *negligibly small fractional longitudinal velocity change assumption*: $\Delta v_z/v_z(0) \approx 0$).

C. The textbook model understanding

Since $z_0 = v_z t$, where $v_z = \text{const}$, the phasor's transverse components in the paraxial approximation (4) can

be presented as

$$\begin{aligned} \tilde{E}_x(z_0) &= \tilde{E}_\perp(z_0) \cos(\tilde{\omega}_c(t)t), \\ \tilde{E}_y(z_0) &= \tilde{E}_\perp(z_0) \sin(\tilde{\omega}_c(t)t), \end{aligned} \quad (9)$$

where $\tilde{E}_\perp(z_0) = \sqrt{\tilde{E}_x^2(z_0) + \tilde{E}_y^2(z_0)}$ is the magnitude of transverse phasor or just transverse phasor field, which depends on the electron's z coordinate in axis of helix and is rotating, $\tilde{\omega}_c(t) = \arctan(\tilde{E}_y(t)/\tilde{E}_x(t))/t$ is time-dependent natural frequency of the system or the frequency of rotation of the field. Thus, the field is frequency- and amplitude-modulated circularly polarized¹, since the frequency is time-dependent (frequency-modulated): $\tilde{\omega}_c(t)$ and the magnitude is space-dependent (amplitude-modulated): $\tilde{E}_\perp(z_0)$.

According to the *textbook model*, the equations of motion inside the helical deflector can be effectively described as

$$\begin{aligned} \dot{v}_x &\approx -\frac{e}{m\gamma} \tilde{E}_\perp \cos(\omega_c t) \sin(\omega t + \phi) \theta(\tau - t) \theta(t), \\ \dot{v}_y &\approx -\frac{e}{m\gamma} \tilde{E}_\perp \sin(\omega_c t) \sin(\omega t + \phi) \theta(\tau - t) \theta(t), \\ \dot{v}_z &\approx 0, \end{aligned} \quad (10)$$

Due to our *capacitor model* and description of the electric field as (9), we understand the *textbook model* as following. The transverse phasor field is considered with constant magnitude \tilde{E}_\perp and constant frequency $\omega_c = \frac{2\pi v_z}{\lambda_c}$ (natural frequency of a system), hence is simply circularly polarized. In that case, the equations of motion (8) can be solved analytically. In the next section sine $\sin x$ and cosine $\cos x$ functions are denoted as s_x and c_x , where x is an argument.

We perform a numerical comparison between our *capacitor model* and the corresponding *textbook model* (see, for example, Figs. 2 and 3). For large values of κ (in our case, already for $\kappa \geq 6/\pi$ or $\lambda/R \geq 12$, see Figs. 2 and 3), the *textbook model* provides a valid approximation. However, the final and approximated values of the field parameters were not specified in his original formulation in the textbook. We claim that the following approximation holds, i.e, the electric field is approximated by its central value:

$$\begin{aligned} \tilde{E}_\perp(t) &\approx \tilde{E}_\perp(t = \tau/2), \\ \tilde{\omega}_c(t) &\approx \omega_c, \end{aligned} \quad (11)$$

where $\tau/2$ represents the central value of the temporal range, which is truncated $([0, \tau])$ using the Heaviside step functions $\theta(x)$. The endpoint $\tau = \frac{R\kappa(\varphi_2 - \varphi_1)}{v_z}$ is derived from the condition $\Delta z = R\kappa\Delta\varphi$. The use of Heaviside truncation in the *textbook model* is natural, as it defines the temporal bounds of the field.

¹ Also can be called *helically polarized* due to the field's trajectory when electron is passing through the helical deflector.

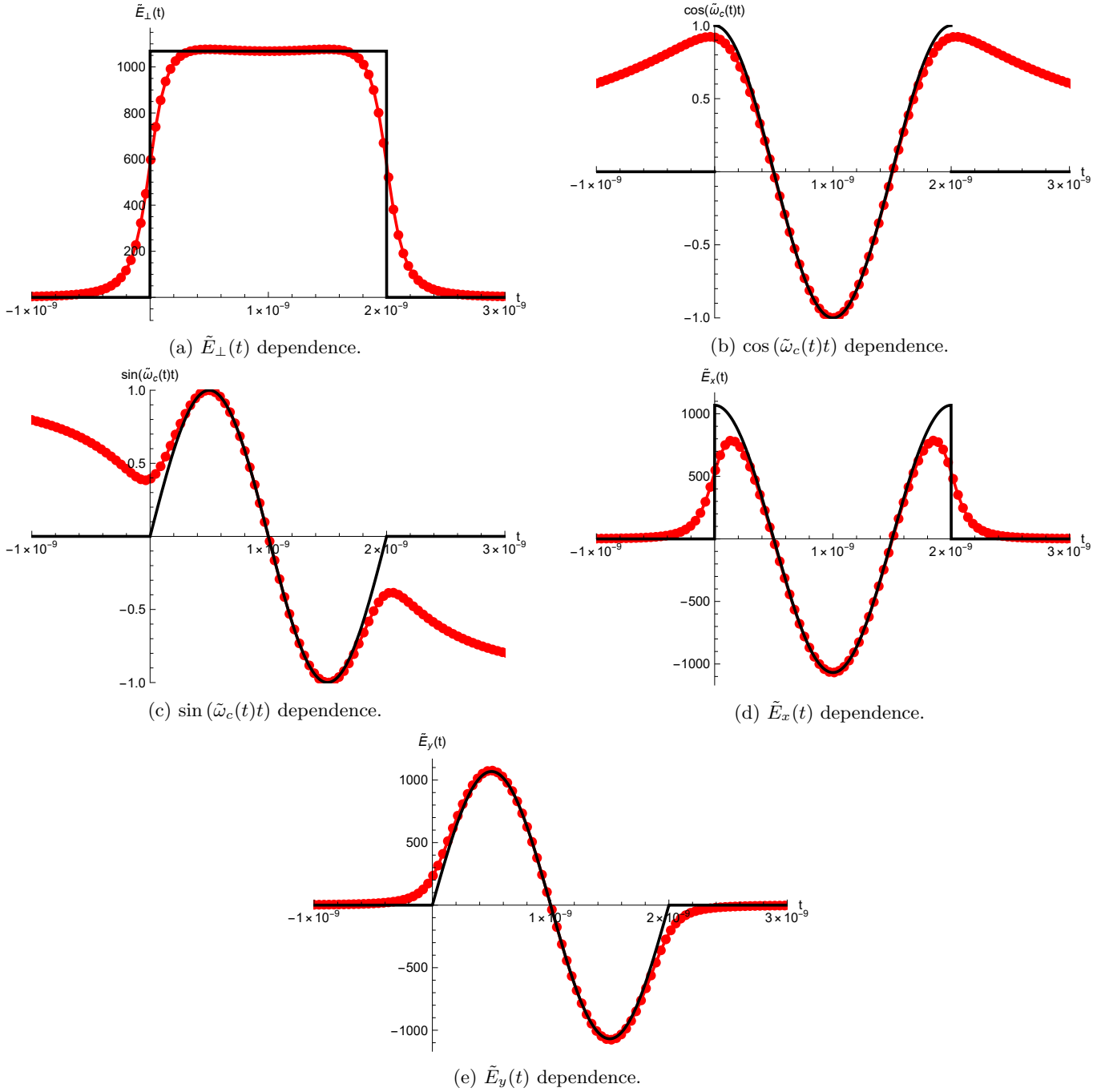


FIG. 2: A capacitor model [paraxial approximation] (red) and its approximation yielding the textbook model (black) for the case $\kappa = 6/\pi$ and $n = 1$ (see Table I).

III. DEFLECTOR'S ELLIPSE SIZES ON A SCREEN

A. Theory case

Integration of equations of motion (8) for our theory gives velocities and coordinates in the transverse plane

$$\begin{aligned}
 v_x &= A'_1 c_\phi + B'_1 s_\phi, \\
 v_y &= A'_2 c_\phi + B'_2 s_\phi, \\
 x &= a_1 c_\phi + b_1 s_\phi, \\
 y &= a_2 c_\phi + b_2 s_\phi, \\
 A'_1 &= -\frac{e}{m\gamma} \int_0^\tau \tilde{E}_x(t) s_{\omega t} dt, \\
 B'_1 &= -\frac{e}{m\gamma} \int_0^\tau \tilde{E}_x(t) c_{\omega t} dt, \\
 A'_2 &= -\frac{e}{m\gamma} \int_0^\tau \tilde{E}_y(t) s_{\omega t} dt, \\
 B'_2 &= -\frac{e}{m\gamma} \int_0^\tau \tilde{E}_y(t) c_{\omega t} dt, \\
 a_1 &= -\frac{e}{m\gamma} \int_0^\tau \int_0^{\tau'} \tilde{E}_x(t) s_{\omega t} dt d\tau', \\
 b_1 &= -\frac{e}{m\gamma} \int_0^\tau \int_0^{\tau'} \tilde{E}_x(t) c_{\omega t} dt d\tau', \\
 a_2 &= -\frac{e}{m\gamma} \int_0^\tau \int_0^{\tau'} \tilde{E}_y(t) s_{\omega t} dt d\tau', \\
 b_2 &= -\frac{e}{m\gamma} \int_0^\tau \int_0^{\tau'} \tilde{E}_y(t) c_{\omega t} dt d\tau'.
 \end{aligned} \tag{12}$$

The coordinates $X(\tau_D, \tau) \triangleq x(\tau) + X'(\tau_D, \tau)$ and $Y(\tau_D, \tau) \triangleq y(\tau) + Y'(\tau_D, \tau)$ of an electron on the screen, where $X'(\tau_D, \tau) = v_x(\tau)\tau_D$ and $Y'(\tau_D, \tau) = v_y(\tau)\tau_D$, will be

$$\begin{aligned}
 X &= A_1 c_\phi + B_1 s_\phi, \\
 Y &= A_2 c_\phi + B_2 s_\phi, \\
 A_1 &= a_1 + A'_1 \tau_D, \\
 B_1 &= b_1 + B'_1 \tau_D, \\
 A_2 &= a_2 + A'_2 \tau_D, \\
 B_2 &= b_2 + B'_2 \tau_D,
 \end{aligned} \tag{13}$$

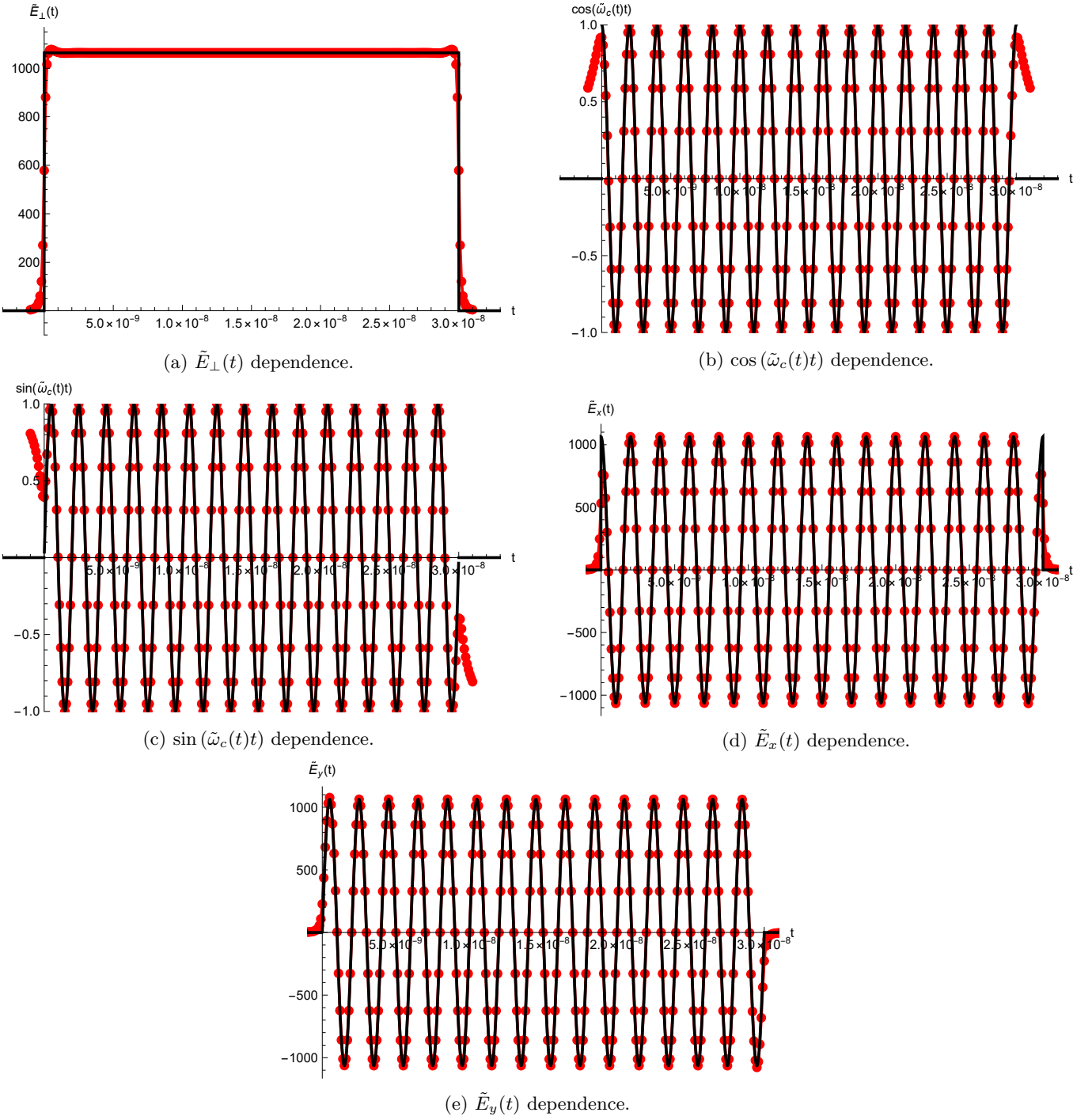


FIG. 3: A capacitor model [paraxial approximation] (red) and its approximation yielding the textbook model (black) for the case $\kappa = 6/\pi$ (see Table I) but $n = 15$ ($l = 15 \times 60 \text{ mm} = 90 \text{ cm}$).

Let's rewrite the equations for coordinates from (12) in the form of a single equation of conic sections

$$aX^2 + bXY + cY^2 - 1 = 0,$$

$$a = \frac{\alpha}{A_1^2} + \frac{\beta}{B_1^2}, b = -2 \left(\frac{\alpha}{A_1 A_2} + \frac{\beta}{B_1 B_2} \right), c = \frac{\alpha}{A_2^2} + \frac{\beta}{B_2^2},$$

$$\alpha = \frac{1}{\left(\frac{B_1}{A_1} - \frac{B_2}{A_2} \right)^2}, \quad \beta = \frac{1}{\left(\frac{A_1}{B_1} - \frac{A_2}{B_2} \right)^2}. \quad (14)$$

After doing rotation of the coordinate frame

$$\begin{bmatrix} X \\ Y \end{bmatrix} = \begin{bmatrix} c_\theta & -s_\theta \\ s_\theta & c_\theta \end{bmatrix} \begin{bmatrix} x' \\ y' \end{bmatrix}, \quad (15)$$

one can find equation $a'(x')^2 + c'(y')^2 = 1$ corresponding to the equation of the ellipse in rotated coordinates. Modifying the equation to the standard one $\frac{(x')^2}{\chi^2} + \frac{(y')^2}{\varkappa^2} = 1$, one can simply find the rotation angle θ and the sizes χ and \varkappa for rotated ellipse

$$\begin{aligned} \chi &= \sqrt{\frac{2}{(a-c)c_{2\theta} + bs_{2\theta} + a + c}}, \\ \varkappa &= \sqrt{\frac{2}{(c-a)c_{2\theta} - bs_{2\theta} + a + c}}, \\ \chi - \varkappa &= 4 \frac{(a-c)c_{2\theta} + bs_{2\theta}}{(\chi + \varkappa)(a'_0 + b'_0 c_{4\theta} + c'_0 s_{4\theta})}, \\ s_{2\theta} &= \frac{b}{\sqrt{(a-c)^2 + b^2}}, \\ c_{2\theta} &= \frac{a-c}{\sqrt{(a-c)^2 + b^2}}, \\ a'_0 &= a^2 - b^2 + c^2 + 6ac, \\ b'_0 &= b^2 - a^2 - c^2 + 2ac, \\ c'_0 &= bc - ab, \\ \theta &= \frac{1}{2} \arctan \left(\frac{b}{a-c} \right), \quad \theta \in \left(-\frac{\pi}{2}, \frac{\pi}{2} \right). \end{aligned} \quad (16)$$

Since θ is a rotation angle, which is necessary to map rotated plane to unrotated one, i.e., after the rotation of the rotated ellipse by this angle we get unrotated ellipse, the rotation angle of the rotated ellipse is actually $-\theta$, because the computational coordinate system is (x', y') .

Length of the ellipse line from the initial phase ϕ_1 to

the final ϕ_2 is

$$s = \int_{X(\phi_1)}^{X(\phi_2)} \sqrt{1 + \left(\frac{dY}{dX} \right)^2} dx = \quad (17a)$$

$$= \int_{\phi_1}^{\phi_2} \sqrt{\left(\frac{dr(\phi)}{d\phi} \right)^2 + (r(\phi))^2} d\phi = \quad (17b)$$

$$= \int_{\phi_1}^{\phi_2} \sqrt{\left(\frac{dX}{d\phi} \right)^2 + \left(\frac{dY}{d\phi} \right)^2} d\phi = \quad (17c)$$

$$= \int_{\phi_1}^{\phi_2} \sqrt{A_0 + B_0 c_{2\phi} - C_0 s_{2\phi}} d\phi = \quad (17d)$$

$$= \int_{\phi_1}^{\phi_2} \sqrt{A_0 - D_0 s_{2\phi - \alpha_0}} d\phi, \quad (17e)$$

$$(17f)$$

where $A_0 = (A_1^2 + A_2^2 + B_1^2 + B_2^2)/2$, $B_0 = (B_1^2 + B_2^2 - A_1^2 - A_2^2)/2$, $C_0 = A_1 B_1 + A_2 B_2$, $D_0 = \sqrt{B_0^2 + C_0^2}$, $\alpha_0 = \arctan(B_0/C_0)$.

B. Textbook model case

Integration of equations of motion (10) for the *textbook model*, subject to the initial conditions $v_x(0) = v_y(0) = x(0) = y(0) = 0$, corresponding to an *idealized zero-emittance, space-charge-free* (mutual Coulomb interactions between charges are neglected) or *single-charge pencil beam*, yields the following velocities and coordi-

nates in the transverse plane

$$v_x(\tau) = \frac{1}{2}A(\tilde{E}_\perp) \left(\frac{c_\phi}{\omega - \omega_c} + \frac{c_\phi}{\omega + \omega_c} - \frac{c_{\phi+\tau(\omega-\omega_c)}}{\omega - \omega_c} - \frac{c_{\phi+\tau(\omega+\omega_c)}}{\omega + \omega_c} \right) \quad (18a)$$

$$v_y(\tau) = \frac{1}{2}A(\tilde{E}_\perp) \left(-\frac{s_\phi}{\omega - \omega_c} + \frac{s_\phi}{\omega + \omega_c} + \frac{s_{\phi+\tau(\omega-\omega_c)}}{\omega - \omega_c} - \frac{s_{\phi+\tau(\omega+\omega_c)}}{\omega + \omega_c} \right) \quad (18b)$$

$$x(\tau) = \frac{1}{2}A(\tilde{E}_\perp) \left(\frac{\tau c_\phi}{\omega - \omega_c} + \frac{\tau c_\phi}{\omega + \omega_c} + \frac{s_\phi}{(\omega - \omega_c)^2} + \frac{s_\phi}{(\omega + \omega_c)^2} - \frac{s_{\phi+\tau(\omega-\omega_c)}}{(\omega - \omega_c)^2} - \frac{s_{\phi+\tau(\omega+\omega_c)}}{(\omega + \omega_c)^2} \right) \quad (18c)$$

$$y(\tau) = \frac{1}{2}A(\tilde{E}_\perp) \left(-\frac{\tau s_\phi}{\omega - \omega_c} + \frac{\tau s_\phi}{\omega + \omega_c} + \frac{c_\phi}{(\omega - \omega_c)^2} - \frac{c_\phi}{(\omega + \omega_c)^2} - \frac{c_{\phi+\tau(\omega-\omega_c)}}{(\omega - \omega_c)^2} + \frac{c_{\phi+\tau(\omega+\omega_c)}}{(\omega + \omega_c)^2} \right), \quad (18d)$$

where $A(\tilde{E}_\perp) = -\frac{e}{m\gamma}\tilde{E}_\perp$ and τ is TOF of an electron inside the deflector. Introducing the standard *textbook notations* $x_1 = (\omega_c - \omega)\tau/2$ and $x_2 = (\omega_c + \omega)\tau/2$, the transverse velocities and transverse coordinates can be expressed as

]

$$v_x(\tau) = \frac{1}{2}A(\tilde{E}_\perp)\tau \left(-\frac{\sin x_1}{x_1} \sin(x_1 - \phi) + \frac{\sin x_2}{x_2} \sin(x_2 + \phi) \right), \quad (19a)$$

$$v_y(\tau) = \frac{1}{2}A(\tilde{E}_\perp)\tau \left(\frac{\sin x_1}{x_1} \cos(x_1 - \phi) - \frac{\sin x_2}{x_2} \cos(x_2 + \phi) \right), \quad (19b)$$

$$x(\tau) = \frac{1}{4}A(\tilde{E}_\perp)\tau^2 \left(\cos\phi \left(-\frac{1}{x_1} \left(1 - \frac{\sin 2x_1}{2x_1} \right) + \frac{1}{x_2} \left(1 - \frac{\sin 2x_2}{2x_2} \right) \right) + \sin\phi \left(\frac{\sin^2 x_1}{x_1^2} + \frac{\sin^2 x_2}{x_2^2} \right) \right), \quad (19c)$$

$$y(\tau) = \frac{1}{4}A(\tilde{E}_\perp)\tau^2 \left(\cos\phi \left(\frac{\sin^2 x_1}{x_1^2} - \frac{\sin^2 x_2}{x_2^2} \right) + \sin\phi \left(\frac{1}{x_1} \left(1 - \frac{\sin 2x_1}{2x_1} \right) + \frac{1}{x_2} \left(1 - \frac{\sin 2x_2}{2x_2} \right) \right) \right) \quad (19d)$$

]

Transverse coordinates on the screen follow as

$$X(\phi) = A_1 c_\phi + B_1 s_\phi, \quad (20a)$$

$$Y(\phi) = A_2 c_\phi + B_2 s_\phi, \quad (20b)$$

$$A_1 = \frac{1}{2} \frac{A(\tilde{E}_\perp)}{(\omega^2 - \omega_c^2)^2} \left(C_0^{A_1} + C_+^{A_1} c_{\tau(\omega+\omega_c)} + S_+^{A_1} s_{\tau(\omega+\omega_c)} + C_-^{A_1} c_{\tau(\omega-\omega_c)} + S_-^{A_1} s_{\tau(\omega-\omega_c)} \right), \quad (20c)$$

$$C_0^{A_1} = 2(\tau + \tau_D)\omega(\omega^2 - \omega_c^2),$$

$$C_+^{A_1} = -\tau_D(\omega - \omega_c)^2(\omega + \omega_c),$$

$$S_+^{A_1} = -(\omega - \omega_c)^2,$$

$$C_-^{A_1} = -\tau_D(\omega - \omega_c)(\omega + \omega_c)^2,$$

$$S_-^{A_1} = -(\omega + \omega_c)^2,$$

$$B_1 = \frac{1}{2} \frac{A(\tilde{E}_\perp)}{(\omega^2 - \omega_c^2)^2} \left(C_0^{B_1} + C_+^{B_1} c_{\tau(\omega+\omega_c)} + S_+^{B_1} s_{\tau(\omega+\omega_c)} + C_-^{B_1} c_{\tau(\omega-\omega_c)} + S_-^{B_1} s_{\tau(\omega-\omega_c)} \right), \quad (20d)$$

$$C_0^{B_1} = 2(\omega^2 + \omega_c^2),$$

$$C_+^{B_1} = -(\omega - \omega_c)^2,$$

$$S_+^{B_1} = \tau_D(\omega - \omega_c)^2(\omega + \omega_c),$$

$$C_-^{B_1} = -(\omega + \omega_c)^2,$$

$$S_-^{B_1} = \tau_D(\omega - \omega_c)(\omega + \omega_c)^2,$$

$$A_2 = \frac{1}{2} \frac{A(\tilde{E}_\perp)}{(\omega^2 - \omega_c^2)^2} \left(C_0^{A_2} + C_+^{A_2} c_{\tau(\omega+\omega_c)} + S_+^{A_2} s_{\tau(\omega+\omega_c)} + C_-^{A_2} c_{\tau(\omega-\omega_c)} + S_-^{A_2} s_{\tau(\omega-\omega_c)} \right), \quad (20e)$$

$$C_0^{A_2} = 4\omega\omega_c,$$

$$C_+^{A_2} = (\omega - \omega_c)^2,$$

$$S_+^{A_2} = -\tau_D(\omega - \omega_c)^2(\omega + \omega_c), \quad (20f)$$

$$C_-^{A_2} = -(\omega + \omega_c)^2,$$

$$S_-^{A_2} = \tau_D(\omega - \omega_c)(\omega + \omega_c)^2,$$

$$B_2 = \frac{1}{2} \frac{A(\tilde{E}_\perp)}{(\omega^2 - \omega_c^2)^2} \left(C_0^{B_2} + C_+^{B_2} c_{\tau(\omega+\omega_c)} + S_+^{B_2} s_{\tau(\omega+\omega_c)} + C_-^{B_2} c_{\tau(\omega-\omega_c)} + S_-^{B_2} s_{\tau(\omega-\omega_c)} \right), \quad (20g)$$

$$C_0^{B_2} = -2(\tau + \tau_D)\omega_c(\omega^2 - \omega_c^2),$$

$$C_+^{B_2} = -\tau_D(\omega - \omega_c)^2(\omega + \omega_c),$$

$$S_+^{B_2} = -(\omega - \omega_c)^2,$$

$$C_-^{B_2} = \tau_D(\omega - \omega_c)(\omega + \omega_c)^2,$$

$$S_-^{B_2} = (\omega + \omega_c)^2,$$

where τ_D is TOF of an electron outside the deflector, between the deflector and the screen.

$$v_x(\phi) = A'_1 c_\phi + B'_1 s_\phi, \quad (21a)$$

$$v_y(\phi) = A'_2 c_\phi + B'_2 s_\phi, \quad (21b)$$

$$A'_1 = \frac{1}{2} \frac{A(\tilde{E}_\perp)}{(\omega^2 - \omega_c^2)} (F_0 - F_- c_{\tau(\omega+\omega_c)} - F_+ c_{\tau(\omega-\omega_c)}), \quad (21c)$$

$$B'_1 = \frac{1}{2} \frac{A(\tilde{E}_\perp)}{(\omega^2 - \omega_c^2)} (F_- s_{\tau(\omega+\omega_c)} + F_+ s_{\tau(\omega-\omega_c)}), \quad (21d)$$

$$A'_2 = \frac{1}{2} \frac{A(\tilde{E}_\perp)}{(\omega^2 - \omega_c^2)} (-F_- s_{\tau(\omega+\omega_c)} + F_+ s_{\tau(\omega-\omega_c)}), \quad (21e)$$

$$B'_2 = \frac{1}{2} \frac{A(\tilde{E}_\perp)}{(\omega^2 - \omega_c^2)} (-F_c - F_- c_{\tau(\omega+\omega_c)} + F_+ c_{\tau(\omega-\omega_c)}), \quad (21f)$$

$$F_0 = 2\omega,$$

$$F_c = 2\omega_c,$$

$$F_- = \omega - \omega_c,$$

$$F_+ = \omega + \omega_c,$$

IV. LIMIT

In the resonance limit, $\omega \rightarrow \omega_c$, the TOF required for a charged particle to complete one turn ($n = 1$) is equal to the period of the applied RF voltage. For the calculation of the deflection amplitudes and the rotation angle on the resonance $\omega \rightarrow \omega_c$, the following notation will be used

$$a_c = 2\tau\omega_c = 4\pi n, \quad (22a)$$

$$a_D = 2\tau_D\omega_c = 4\pi n_D, \quad (22b)$$

where the deflector parameter $n = \frac{l}{\lambda}$ is the number of turns of a helix, $n_D = \frac{L}{\lambda}$ is the number of *phantom* turns of a helix imagined between the end of the deflector and the screen.

A. TOF in a deflector

In the limit $\omega \rightarrow \omega_c \Rightarrow \{x \rightarrow x_c, y \rightarrow y_c\}$

$$\begin{aligned} x_c &= a_{1c} c_\phi + b_{1c} s_\phi, \\ y_c &= a_{2c} c_\phi + b_{2c} s_\phi, \\ a_{1c} &= b_{2c} = \frac{A(\tilde{E}_\perp)}{8\omega_c^2} (a_c - \sin a_c), \\ a_{2c} &= \frac{A(\tilde{E}_\perp)}{8\omega_c^2} \left(\frac{a_c^2}{2} + 1 - \cos a_c \right), \\ b_{1c} &= \frac{A(\tilde{E}_\perp)}{8\omega_c^2} \left(\frac{a_c^2}{2} - (1 - \cos a_c) \right). \end{aligned} \quad (23)$$

The sizes of the small ellipse are the following

$$\begin{aligned} \tilde{\chi}_c &= \frac{|A(\tilde{E}_\perp)|}{16\omega_c^2} (a_c^2 - 2\sqrt{g(a_c)}) = \frac{l^2 |A(\tilde{E}_\perp)|}{v_z^2} \tilde{G}_1(n), \\ \tilde{\varkappa}_c &= \frac{|A(\tilde{E}_\perp)|}{16\omega_c^2} (a_c^2 + 2\sqrt{g(a_c)}) = \frac{l^2 |A(\tilde{E}_\perp)|}{v_z^2} \tilde{G}_2(n), \\ \tilde{G}_1(n) &= \frac{1}{4} \left(1 - \frac{\sqrt{g(n)}}{8\pi^2 n^2} \right), \\ \tilde{G}_2(n) &= \frac{1}{4} \left(1 + \frac{\sqrt{g(n)}}{8\pi^2 n^2} \right), \\ g(a_c) &= 2 + a_c^2 - 2 \cos a_c - 2a_c \sin a_c, \\ g(n) &= 2 + 16\pi^2 n^2 - 2 \cos(4\pi n) - 8\pi n \sin(4\pi n), \end{aligned} \quad (24)$$

where $a_c^2 - 2\sqrt{g(a_c)} \geq 0$, since the function $h(a_c) = a_c^4 - 4g(a_c) \geq 0$, which can be proved by the change of the variable $u = a_c/2$ and the study of its behavior $h(u) = 16(u^4 - (u - \sin u \cos u)^2 - \sin^4 u) \geq 0$.

$\tilde{G}_1(n)$ and $\tilde{G}_2(n)$ profiles from the number of turns are monotonically increasing and decreasing functions (see Fig. 4), respectively:

- for tiny number of turns, $\tilde{G}_1(n)$ profile has its minimum and $\tilde{G}_2(n)$ its maximum:

$$\begin{aligned} \tilde{G}_{1,\min}(n) &= \lim_{n \rightarrow 0} \tilde{G}_1(n) = 0, \\ \tilde{G}_{2,\max}(n) &= \lim_{n \rightarrow 0} \tilde{G}_2(n) = \frac{1}{2}, \end{aligned} \quad (25)$$

- when for large number of turns they get closer

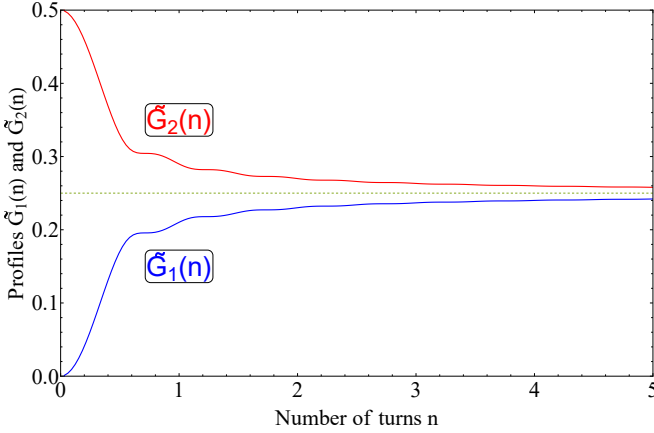


FIG. 4: $\tilde{G}_1(n)$ and $\tilde{G}_2(n)$ profile dependences on the number of turns n (the small ellipse).

$$(\tilde{G}_{1,\max}(n) = \tilde{G}_{2,\max}(n) = 1/4):$$

$$\begin{aligned} \tilde{G}_{1,\max}(n) &= \lim_{n \rightarrow \infty} \tilde{G}_1(n) = \frac{1}{4}, \\ \tilde{G}_{2,\min}(n) &= \lim_{n \rightarrow \infty} \tilde{G}_2(n) = \frac{1}{4}, \end{aligned} \quad (26)$$

and that case corresponds to the case when the ellipse gets closer to the circle $\tilde{\chi}_c \rightarrow \tilde{\chi}_c$ with a radius:

$$\tilde{r}_c = \frac{l^2 |A(\tilde{E}_\perp)|}{4v_z^2}. \quad (27)$$

The *paraxial approximation* holds when $\tilde{\chi}_c \ll R$ ($\sqrt{x^2(\phi) + y^2(\phi)} \ll d/2$):

$$\frac{e\tilde{E}_\perp}{m\gamma} \frac{l^2}{v_z^2} \tilde{G}_2(n) \ll R, \quad (28)$$

therefore, the *textbook model* and consequences (derived formulas) are true only when (28) holds. So, to get a circle, experimentalists must simultaneously ensure that approximations in Sec. II, condition (28), largeness of n , and Shamaev conditions.

From the validity of the *approximation yielding the textbook model* ($\lambda/R \geq 12$) [see (11) and (10)] and the *paraxial approximation* of the *capacitor model* (28), one gets the following two competitive conditions

$$12ln \leq \frac{l^2}{R} \ll \frac{v_z^2}{\tilde{G}_2(n)} \frac{m\gamma}{e\tilde{E}_\perp}. \quad (29)$$

In the limit $\omega \rightarrow \omega_c$, the angle of the first ellipse (see Fig. 5) is equal to

$$\theta_1 = \frac{1}{2} \arctan \left(\frac{a_c - \sin a_c}{\cos a_c - 1} \right), \quad (30)$$

which has its extrema at $n \rightarrow 0$

$$\theta_{1,\max} = \lim_{n \rightarrow 0} \theta_1(n) = 0, \quad (31)$$

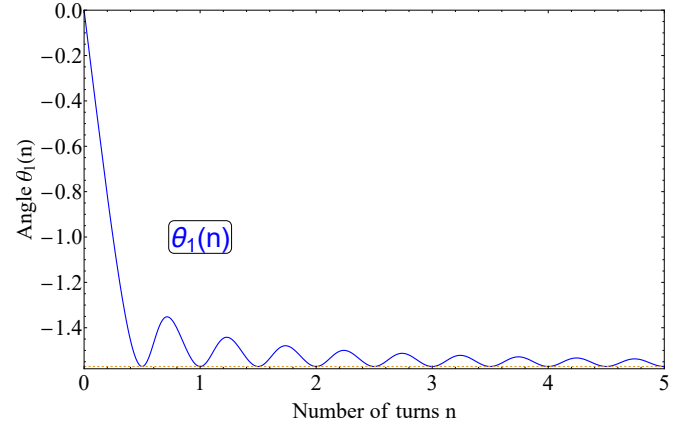


FIG. 5: Angle $\theta_1(n)$ dependence on the number of turns n (the small ellipse).

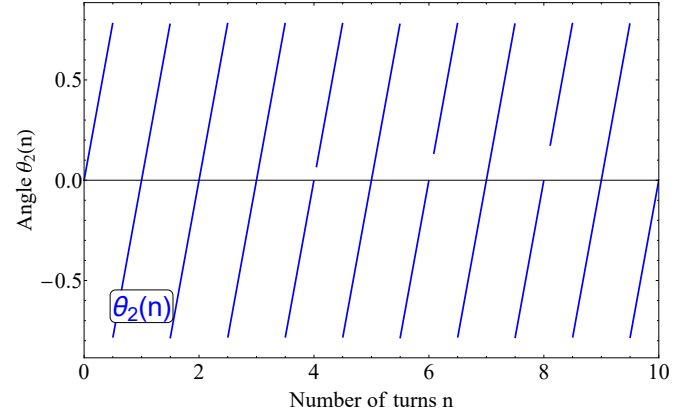


FIG. 6: Angle $\theta_2(n)$ dependence on the number of turns n (the large ellipse).

and at $n \rightarrow k + 1/2$, $k \in \mathbb{N}_0$ and $n \rightarrow \infty$

$$\theta_{1,\min} = \lim_{n \rightarrow k+1/2} \theta_1(n) = \lim_{n \rightarrow \infty} \theta_1(n) = -\frac{\pi}{2}. \quad (32)$$

B. TOF between a deflector and a screen

In the limit $\omega \rightarrow \omega_c \Rightarrow \{X' \rightarrow X'_c, Y' \rightarrow Y'_c\}$

$$\begin{aligned} X'_c &= \tau_D (A'_{1c} c_\phi + B'_{1c} s_\phi) = a'_{1c} c_\phi + b'_{1c} s_\phi = \\ &= A'_{xc} \cos(\phi + \phi'_{xc}), \end{aligned}$$

$$\begin{aligned} Y'_c &= \tau_D (A'_{2c} c_\phi + B'_{2c} s_\phi) = a'_{2c} c_\phi + b'_{2c} s_\phi = \\ &= A'_{yc} \sin(\phi + \phi'_{yc}), \end{aligned}$$

$$a'_{1c} = b'_{2c} = \frac{A(\tilde{E}_\perp)}{8\omega_c^2} (1 - \cos a_c) a_D, \quad (33)$$

$$b'_{1c} = \frac{A(\tilde{E}_\perp)}{8\omega_c^2} (a_c + \sin a_c) a_D,$$

$$a'_{2c} = \frac{A(\tilde{E}_\perp)}{8\omega_c^2} (a_c - \sin a_c) a_D.$$

The sizes of the big ellipse are the following

$$\chi'_c = \frac{|A(\tilde{E}_\perp)|}{8\omega_c^2} \frac{|a_c^2 - 2(1 - \cos a_c)|}{((a_c^2 + 2(1 - \cos a_c)) + 2\sqrt{2}a_c\sqrt{1 - \cos a_c})^{1/2}} a_D = \frac{|A(\tilde{E}_\perp)|}{8\omega_c^2} a_D a_c \left(1 - \left| \frac{\sin(a_c/2)}{a_c/2} \right| \right), \quad (34a)$$

$$\varkappa'_c = \frac{|A(\tilde{E}_\perp)|}{8\omega_c^2} \frac{|a_c^2 - 2(1 - \cos a_c)|}{((a_c^2 + 2(1 - \cos a_c)) - 2\sqrt{2}a_c\sqrt{1 - \cos a_c})^{1/2}} a_D = \frac{|A(\tilde{E}_\perp)|}{8\omega_c^2} a_D a_c \left(1 + \left| \frac{\sin(a_c/2)}{a_c/2} \right| \right), \quad (34b)$$

where the final formulas in (34a) and (34b) exactly correspond to the ones in the book [1] (note that in the book $n = 1$).

In the limit $\omega \rightarrow \omega_c$, the angle of the second ellipse (see Fig. 6) is equal to

$$\begin{aligned} \theta_2 &= \frac{1}{2} \arctan \left(\tan \frac{a_c}{2} \right) = \frac{a_c}{4} - \frac{\pi}{2} \left[\frac{1}{2} \left\lceil \frac{a_c}{\pi} \right\rceil \right] = \\ &= \pi n - \frac{\pi}{2} \left[\frac{1}{2} \left\lfloor 4n \right\rfloor \right], \end{aligned} \quad (35)$$

where, to restrict θ_2 to the first quadrant, the ceiling $\lceil \cdot \rceil$ and the floor $\lfloor \cdot \rfloor$ rounding functions are used. This is a mathematical convention and in physics it is usually more natural to use rotation angle which is continuous function of n , i.e., $\theta_2 = \pi n$.

Hereby, the Shamaev conditions to get a circle simply can be seen: when the following

1. Shamaev resonance $\omega \rightarrow \omega_c$, i.e., the equality of the TOF ($\tau_c = \frac{\lambda}{v_z} = \frac{2\pi}{\omega_c}$) of a charged particle through one turn of the helix to the period ($T = \frac{2\pi}{\omega}$) of the high-frequency voltage: $\tau_c = T$,
2. a half-integer number of turns $n = k/2$ ($a_c/2 = 2\pi k$), $k \in \mathbb{N}$, which is equivalent to $\tau = \frac{\pi k}{\omega_c}$ written in the book, [1]

hold, the big ellipse turns to a circle ($\chi'_c = \varkappa'_c$) with a radius

$$r'_c = \frac{|A(\tilde{E}_\perp)|}{8\omega_c^2} a_c a_D = \frac{e\tilde{E}_\perp}{m\gamma} \frac{2\pi^2 n n_D}{\omega_c^2} = \frac{e\tilde{E}_\perp}{m\gamma} \frac{lL}{2v_z^2}. \quad (36)$$

C. Total TOF

In the limit $\omega \rightarrow \omega_c \Rightarrow \{X \rightarrow X_c, Y \rightarrow Y_c\}$

$$\begin{aligned} X_c &= A_{1c} c_\phi + B_{1c} s_\phi, \\ Y_c &= A_{2c} c_\phi + B_{2c} s_\phi, \\ A_{1c} &= B_{2c} = \frac{A(\tilde{E}_\perp)}{8\omega_c^2} (a_c - \sin a_c + a_D(1 - \cos a_c)), \\ B_{1c} &= \frac{A(\tilde{E}_\perp)}{8\omega_c^2} \left(\frac{a_c^2}{2} + 1 - \cos a_c + a_D(a_c + \sin a_c) \right), \\ A_{2c} &= \frac{A(\tilde{E}_\perp)}{8\omega_c^2} \left(\frac{a_c^2}{2} + \cos a_c - 1 + a_D(a_c - \sin a_c) \right). \end{aligned} \quad (37)$$

The sizes of the resulting ellipse are the following

$$\chi_c = \frac{|A(\tilde{E}_\perp)|}{16\omega_c^2} \frac{|f_1(a_c, a_D) - k(a_c)|}{\sqrt{k(a_c) + f_2(a_c, a_D) + l(a_c, a_D)}} = \frac{e\tilde{E}_\perp}{m\gamma} \frac{l^2}{4v_z^2} \frac{K_3(n) \left| K_1(n, n_D) - \frac{1}{(4\pi n)^2} \right|}{\sqrt{K_{2+}(n, n_D) + \frac{1}{(4\pi n)^2}}} = \frac{l^2 |A(\tilde{E}_\perp)|}{v_z^2} G_1(n, n_D), \quad (38a)$$

$$\varkappa_c = \frac{|A(\tilde{E}_\perp)|}{16\omega_c^2} \frac{|f_1(a_c, a_D) - k(a_c)|}{\sqrt{k(a_c) + f_2(a_c, a_D) - l(a_c, a_D)}} = \frac{e\tilde{E}_\perp}{m\gamma} \frac{l^2}{4v_z^2} \frac{K_3(n) \left| K_1(n, n_D) - \frac{1}{(4\pi n)^2} \right|}{\sqrt{K_{2-}(n, n_D) + \frac{1}{(4\pi n)^2}}} = \frac{l^2 |A(\tilde{E}_\perp)|}{v_z^2} G_2(n, n_D), \quad (38b)$$

$$l(a_c, a_D) = 4a_c(a_c + 2a_D)\sqrt{2a_D(a_c + a_D)(1 - \cos a_c) + 2(1 - \cos a_c) - 2a_c \sin a_c + a_c^2}, \quad (38c)$$

$$f_1(a_c, a_D) = a_c^4 + 4a_D(a_c + a_D)(2(\cos a_c - 1) + a_c^2), \quad (38d)$$

$$f_2(a_c, a_D) = a_c^4 + 4a_D(a_c + a_D)(2(1 - \cos a_c) + a_c^2), \quad (38e)$$

$$k(a_c) = 8(1 - \cos a_c) - 4a_c(2 \sin a_c - a_c), \quad (38f)$$

$$K_1(n, n_D) = \frac{1 + 4\frac{n_D}{n} \left(1 + \frac{n_D}{n}\right) \left(2\frac{\cos 4\pi n - 1}{(4\pi n)^2} + 1\right)}{8\frac{1 - \cos 4\pi n}{(4\pi n)^2} - 4\left(2\frac{\sin 4\pi n}{4\pi n} - 1\right)}, \quad (38g)$$

$$K_{2\pm}(n, n_D) = \frac{1 + 4\frac{n_D}{n} \left(1 + \frac{n_D}{n}\right) \left(1 + 2\frac{1 - \cos(4\pi n)}{(4\pi n)^2}\right) \pm \tilde{l}(n, n_D)}{8\frac{1 - \cos(4\pi n)}{(4\pi n)^2} - 4\left(2\frac{\sin(4\pi n)}{4\pi n} - 1\right)}, \quad (38h)$$

$$K_3(n) = \sqrt{8\frac{1 - \cos 4\pi n}{(4\pi n)^2} - 4\left(2\frac{\sin 4\pi n}{4\pi n} - 1\right)}, \quad (38i)$$

$$\tilde{l}(n, n_D) = 4 \left(1 + 2\frac{n_D}{n}\right) \sqrt{2\frac{n_D}{n} \left(1 + \frac{n_D}{n}\right) \frac{1 - \cos 4\pi n}{(4\pi n)^2} + 2\frac{1 - \cos 4\pi n}{(4\pi n)^4} - 2\frac{\sin 4\pi n}{(4\pi n)^3} + \frac{1}{(4\pi n)^2}}, \quad (38j)$$

In the limit $\omega \rightarrow \omega_c$, the angle of the final ellipse (see Fig. 9) is equal to

$$\theta_c = \frac{1}{2} \arctan \left(\frac{a_c - \sin a_c + a_D(1 - \cos a_c)}{1 - \cos a_c + a_D \sin a_c} \right). \quad (39)$$

V. TO GET CLOSER TO THE CIRCLE

Although it is written in the book that there is a way to get a circle on the screen, I argue that claim. In the book, it is assumed that electrons are deflected from the deflector's axis at the end of the helical deflector (a full *paraxial approximation*). In reality, if one imagines that the screen is exactly after the deflector, the electrons will be incident to the screen painting a small ellipse, which opposes to the opinion in the book. This small ellipse; since at the end of deflector the transverse radius and the transverse velocity have different directions, i.e., $\tan \alpha \neq \tan \beta$ in general ($\tan \alpha = y(\tau)/x(\tau)$, $\tan \beta = v_y(\tau)/v_x(\tau)$); can drastically change the final ellipse (TOF between screen and the start of deflector), which will be a merging of a small ellipse (TOF at deflector) and a Shamaev ellipse (TOF between screen and the end of deflector). Although the Shamaev ellipse becomes a circle in the case of Shamaev condition (Shamaev res-

onance $\omega \rightarrow \omega_c$ and $\tau = \pi k/\omega_c$ or $n = k/2$, $k \in \mathbb{N}$), the small ellipse is not negligible (compare Forms. (34) and (38)).

VI. ON AND OFF SINGLE-ELECTRON PENCIL BEAM

It will be difficult or ineffective to handle all the mentioned conditions. Therefore, it is important to create a framework to work with the ellipse. The initial equations provide that framework.

Let's imagine that we have *on and off* single-electron pencil beam, which is an approximation of the bunched beam. Contrary to the circle, for this beam of charged particles, their track on the ellipse will be partial ellipse arcs with unequal lengths. The question appears — *How to measure TOF using these unequal lengths?* Experimental answer will be to use RMS (root-mean-square) measure. Probably, RMS of these lengths will provide a relevant measure of time and the final article will touch also this topic.

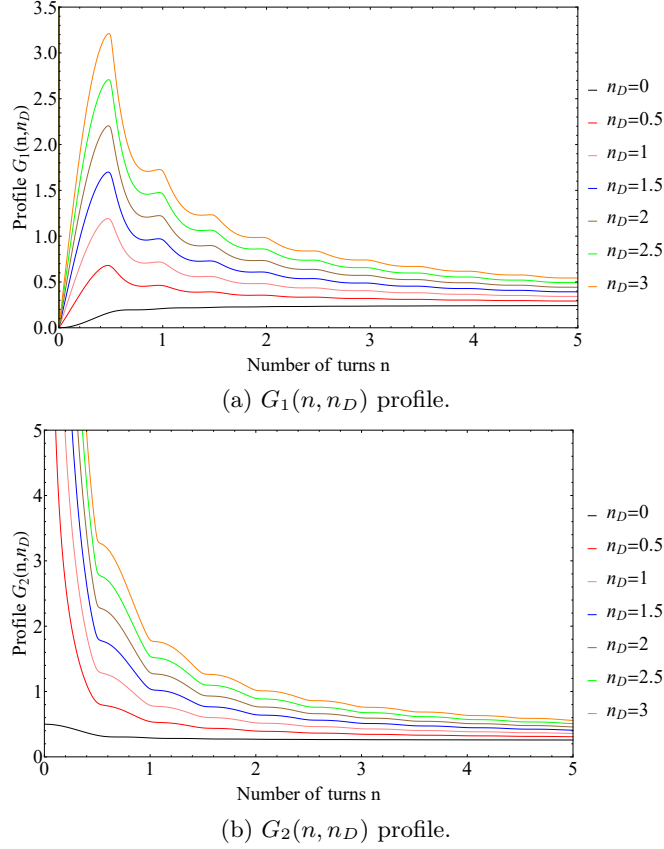


FIG. 7: $G_1(n, n_D)$ and $G_2(n, n_D)$ profile dependences on the number of turns n for the fixed values of the number of phantom turns n_D (the resulting ellipse).

VII. ON THE POSSIBILITY OF MEASURING THE ABSOLUTE ARRIVAL TIME OF THE FIRST CHARGED PARTICLE

Although experimentalists often assume that this device can measure only relative arrival times, I argue that this is not the case. In fact, the device can measure the arrival time of the first charged particle through the initial phase ϕ_0 of the reference field, appearing in the phase relation

$$\phi = \omega \Delta t + \phi_0, \quad (40)$$

where Δt denotes the relative time delay between two charged particles — the first particle and any subsequent one — and ϕ_0 is the initial phase of the reference field at the moment the first particle enters the helical deflector. Experimentally, this phase is equivalent to the time at which the voltage is switched on. Therefore, from an experimental standpoint, the main challenge lies in accurately fixing the times at which the first electron is released and at which the voltage is applied.

VIII. DEFLECTION SENSITIVITY

Let's denote the semi-major and semi-minor axes of the ellipse as

$$r_{\max} = \max\{\chi, \kappa\}, \quad (41a)$$

$$r_{\min} = \min\{\chi, \kappa\}. \quad (41b)$$

Dynamic deflection sensitivity, in the case of the ellipse, ranges in $[S_{\min}(\omega), S_{\max}(\omega)]$, has

1. its maximum as

$$S_{\max}(\omega) = \frac{r_{\max}(\omega)}{U_0 \sin(\omega t)}, \quad (42)$$

2. its minimum as

$$S_{\min}(\omega) = \frac{r_{\min}(\omega)}{U_0 \sin(\omega t)}, \quad (43)$$

3. and its mean as

$$\langle S \rangle = \frac{\sqrt{\chi(\omega) \kappa(\omega)}}{U_0 \sin(\omega t)}, \quad (44)$$

the latter formula is taken according to the mapping of the ellipse to the phantom circle using the

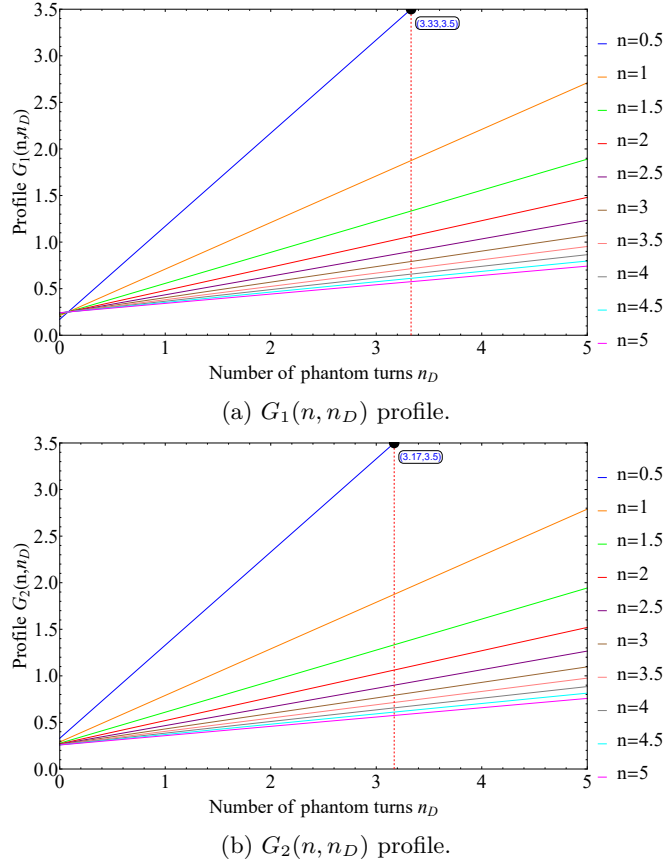


FIG. 8: $G_1(n, n_D)$ and $G_2(n, n_D)$ profile dependences on the phantom number of turns n_D for the fixed values of the number of turns n (the resulting ellipse).

equivalence of their areas $f_e = \pi\chi\varkappa$ and $f = \pi\langle r \rangle^2$, where the radius of that averaged circle is actually a mean deflection $\langle r \rangle = \sqrt{\chi\varkappa}$, representing a geometric mean.

IX. COMMENTS AND CONCLUSIONS

The present article demonstrates that *the textbook model* [1, 2] (and the analogous magnetic-field model [5]) for the helical deflector is actually an approximation of the newly introduced *capacitor model* (with a similar magnetic analogue [21]). In turn, this *capacitor model* should itself be regarded as an approximation [22, 23] to the full electromagnetic theory obtained directly from Maxwell's equations [24, 25]. Furthermore, the capacitor model may deviate from the real electromagnetic behavior because the helical system possesses both capacitance and inductance, whose effective values are frequency dependent in a slow-wave structure. As a result, at a characteristic resonant frequency [26]

$$\omega_{LC} = \frac{1}{\sqrt{LC}} \quad (45)$$

the interaction becomes strongest, and the resulting electric field \tilde{E}_\perp — and hence the deflection amplitude (χ, \varkappa) — achieves its maximum.

In helical slow-wave structures [14–17], \mathbf{E} and \mathbf{B} fields are typically derived from the voltage and current on the transmission line, with the primary goal of analyzing wave propagation along the helix (e.g., phase velocity, dispersion, and impedance). The classical helix slow-wave models used differ from the present case.

In [25], the important problem of deriving the magnetic field of a two-wire helical line from the Poisson equation—and thus directly from Maxwell's equations—was addressed, although only for the constant-current case. A comparable derivation for ribbons or other helical structures — specifically, the determination of the electric field and the full electromagnetic field generated under an applied periodic voltage as a direct solution of Maxwell's equations in full 3D geometry — remains an open problem. Likewise, the resulting deflection characteristics and the validity of *the textbook model* [1, 2] have not yet been fully established. The present article introduces a universal method for deriving the resulting deflection characteristics and addresses questions regarding the validity of *the textbook model* [1, 2] by proposing a new *capacitor model* and their comparison. It establishes

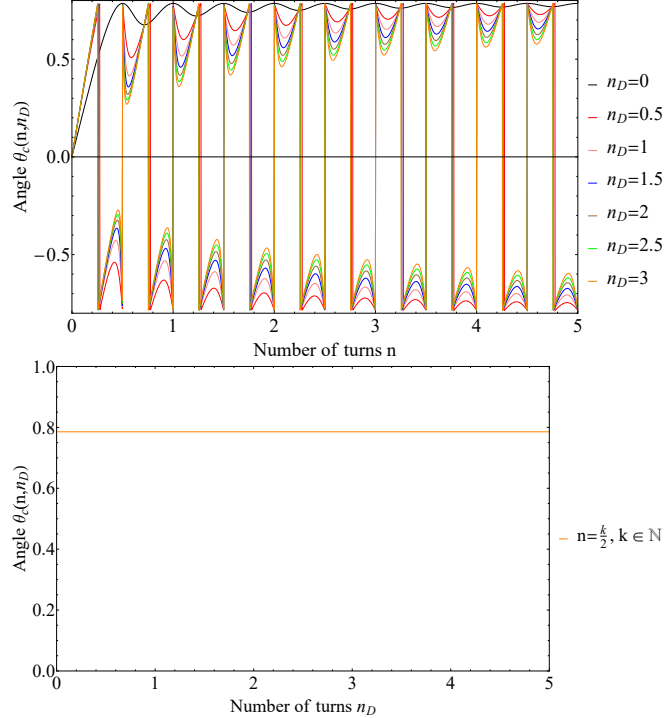


FIG. 9: $\theta_c(n, n_D)$ angle dependences (a) on the number of turns n for the fixed values of the phantom number of turns n_D , and (b) on the phantom number of turns n_D for the fixed values of the number of turns n (the resulting ellipse).

a pathway from modeling to theory for high-precision instruments, such as the Advanced Picosecond Precision Radio Frequency Timer [27].

ACKNOWLEDGMENTS

HLG acknowledges support from the Higher Education and Science Committee of Armenia in the frames of the research project 21AG-1C038 on *Methods of Information Theory in Statistical Physics and Data Science*.

Appendix A: Parameters

Here we present

Appendix B: Magnetic field

An open circuit offers infinite resistance to the flow of current, hence, the amount of current propagating through deflector is due to the time-dependent charge.

So, the current is equal

$$I(t) = 2 \frac{dq(t)}{dt} = -2 \int_0^L \frac{d\rho(t)}{dt} ds = -I_0 \cos(\omega t + \phi), \quad (B1)$$

where, for the parameters I, $I_0 = 2\omega CU_0L = 0.0108608$ A, and $L = 6.7$ cm for $l = 6$ cm ($\lambda = 6$ cm and $n = 1$). The Biot-Savart law gives

$$\mathbf{B}(t) = \mathbf{B}_0 \cos(\omega t + \phi), \quad (B2)$$

$$\mathbf{B}_0 = -\frac{\mu_0}{4\pi} \int \frac{I_0 ds \times \mathbf{r}}{r^3} = \{B_{0x}, B_{0y}, B_{0z}\},$$

hence,

$$B_{0x} = \frac{\mu_0}{4\pi} \int_{\varphi_1}^{\varphi_2} \frac{I_0/R [(\kappa y_0 - z_0 \cos \varphi)/R + \kappa(\varphi \cos \varphi - \sin \varphi)] d\varphi}{S(x_0, y_0, z_0, \varphi)},$$

$$B_{0y} = \frac{\mu_0}{4\pi} \int_{\varphi_1}^{\varphi_2} \frac{I_0/R [-(\kappa x_0 + z_0 \sin \varphi)/R + \kappa(\cos \varphi + \varphi \sin \varphi)] d\varphi}{S(x_0, y_0, z_0, \varphi)},$$

$$B_{0z} = \frac{\mu_0}{4\pi} \int_{\varphi_1}^{\varphi_2} \frac{I_0/R [(x_0 \cos \varphi + y_0 \sin \varphi)/R - 1] d\varphi}{S(x_0, y_0, z_0, \varphi)}. \quad (B3)$$

Let's evaluate a magnetic field. It is approximately equal to $[B] = \frac{\mu_0 I_0}{4\pi R} \approx 2 \times 10^{-7}$ T. His contribution to the Lorentz force will be $\frac{c}{10}[B] \approx 6$ V/m, much smaller than contribution of an electric field $[E] = Q_0/R = 1242.83$ V/m.

TABLE I: Parameters of the helical deflector

U_a	U_0	v_z/c	z_0	R	d	b	l	ϵ_d	$\lambda = l/n$	$\kappa = \lambda/(\pi d)$	φ_1, φ_2	n	ω	L_D
2.5 keV	10 V	1/10	*	$d/2$	10 mm	1.5 mm	60 mm	1	*	*	$-n\pi, n\pi$	1	500 MHz	20 mm

[1] A.A. Zhigarev, *Électronno-Luchevie Pribory (Electron Beam Devices)*, Moscow: Energiya, 1965, p. 199; *Électronnaya Optika i Électronno-Luchevie Pribory (Electron Optics and Electron Beam Devices)*, Moscow: Vysshaya Shkola, 1972, p. 338 (in Russian).

[2] L. Gevorgian, R. Ajvazyan, V. Kakoyan, A. Margaryan, and J. R. M. Annand, “A radio frequency helical deflector for keV electrons,” *Nucl. Instr. Meth. A* **785**, 175–179 (2015).

[3] F.G. Major, “The quantum beat: principles and applications of atomic clocks,” (Springer Science & Business Media, 2007).

[4] H. Ibach, “*The Electron Optics of the Cylindrical Deflector*,” In: *Electron Energy Loss Spectrometers*. Springer Series in Optical Sciences, vol 63. Springer, Berlin, Heidelberg (1991).

[5] A.A. Varfolomeev, *Lazery na svobodnykh elektronakh i perspektivy ikh razvitiya: Obzor* (Lasers on Free Electrons and Prospects for Their Development: Review) (I. V. Kurchatov Institute of Atomic Energy, Moscow, 1980), pp. 13–14.

[6] H.-G. Unger, “Helix waveguide theory and application,” *Bell Syst. Tech. J.* **37**(6), 1599–1647 (1958).

[7] C.-M. Chu, “Propagation of Waves in Helical Wave Guides,” *J. Appl. Phys.* **29**(1), 88–99 (1958).

[8] Z. Menachem and S. Tapuchi, “Wave propagation in a helical waveguide with slab and rectangular dielectric profiles, and applications,” *Prog. Electromagn. Res. B* **34**, 77–102 (2011).

[9] J. Nandi, A.K. Sikdar, P. Das, and A. Ray, “Design of a helical resonator with improved figure of merit,” *Rev. Sci. Instrum.* **93**, 014706 (2022).

[10] K. Deng, Y.L. Sun, W.H. Yuan, Z.T. Xu, J. Zhang, Z.H. Lu, and J. Luo, “A modified model of helical resonator with predictable loaded resonant frequency and Q-factor,” *Rev. Sci. Instrum.* **85**, 104706 (2014).

[11] A. Dyussembayev and D. Psychogiou, “Continuously tunable 3-D printed helical resonators and bandpass filters using actuated liquid metals,” *IEEE Microw. Wirel. Compon. Lett.* **32**(7), 855–858 (2022).

[12] S. Dalarsson, “Analytical and numerical study of helical antennas in radio devices using integral equations,” *B.Sc. thesis* (2015).

[13] Y.D. Chernousov, V. Guidi, P.V. Logachov, L. Tecchio, “Proposal for a detecting system for streak camera with sub-ps resolution and wide dynamic range,” *Nucl. Instr. Meth. A* **451**, 541 (2000).

[14] B.N. Basu, *Electromagnetic theory and applications in beam-wave electronics* (World Scientific, Singapore, 1996).

[15] B.N. Basu, “Dielectric-supported helix in a metal shell,” *Int. J. Electron.* **47**, 311–314 (1979).

[16] J.E. Rowe, *Nonlinear Electron-Wave Interaction Phenomena*, H.G. Booker and N. DeClaris (Ed.), Electrical Science: A Series of Monographs and Texts (Academic Press Inc., New York, 1965).

[17] R.G. Carter, *Microwave and RF vacuum electronic power sources* (Cambridge University Press, Cambridge, 2018).

[18] K.L. Corum and J.F. Corum, “RF coils, helical resonators and voltage magnification by coherent spatial modes,” In *5th International Conference on Telecommunications in Modern Satellite, Cable and Broadcasting Service, TELSIKS 2001*, Proceedings of Papers (Cat. No. 01EX517), vol. 1, pp. 339–348. IEEE, 2001.

[19] E. Martines, R. Cavazzana, L. Cordaro, and M. Zuin, “The helical resonator: A scheme for radio frequency plasma generation,” *Appl. Sci.* **11**, 7444 (2021).

[20] S. Sensiper, “Electromagnetic wave propagation on helical conductors,” *Tech. Rep. №194* (MIT, Cambridge, 1951).

[21] W. R. Smythe, *Static and Dynamic Electricity* (3rd ed.) (Taylor & Francis, Philadelphia, PA, 1989).

[22] O.D. Jefimenko, “Solutions of Maxwell’s equations for electric and magnetic fields in arbitrary media,” *Am. J. Phys.* **60**, 899–902 (1992).

[23] T. Ton, “On the time-dependent, generalized Coulomb and Biot–Savart laws,” *Am. J. Phys.* **59**, 520–528 (1991).

[24] H. Buchholz, *Electrische und magnetische Potentialfelder* (Springer-Verlag, Berlin–Göttingen–Heidelberg, 1957), *Raschet Élektricheskikh i magnitnykh polei* (Izdatel’svo inostrannoi literatury, Moscow, 1961).

[25] L.A. Gevorgian, “Magnetic field inside a two-wire spiral line,” *J. Contemp. Phys.* **57**, 30–35 (2022).

[26] L.A. Gevorgian, *private communication*.

[27] S. Zhamkochyan *et al*, “Advanced picosecond precision Radio Frequency Timer,” *JINST* **19**, C02014 (2024).